

Dose reduction potential in dual-energy subtraction chest radiography based on the relationship between spatial-resolution property and segmentation accuracy of the tumor area

Shu Onodera¹, Yongbum Lee², Tomoyoshi Kawabata¹

¹ Department of Radiology Division of Medical Technology, Tohoku University Hospital, Sendai, Miyagi, Japan

² Graduate School of Health Sciences, Niigata University, Niigata, Japan

ABSTRACT

We investigated the relationship between the spatial-resolution property of soft tissue images and the lesion detection ability using U-net. We aimed to explore the possibility of dose reduction during energy subtraction chest radiography. The correlation between the spatial-resolution property of each dose image and the segmentation accuracy of the tumor area in the four regions where the tumor was placed was evaluated using linear regression analysis. The spatial-resolution property was determined by task-based evaluation, and the task-based modulation transfer function (TTF) was computed as its index. TTFs of the reference dose image and the 75 % dose image showed almost the same frequency characteristics regardless of the location of the tumor, and the Dice coefficient also high. When the tumor was located in the right supraclavicular region and under 50 % dose, the frequency characteristics were significantly reduced, and the Dice coefficient was also low. Our results showed a close relationship between the spatial-resolution property and the segmentation accuracy of tumor area using deep learning in dual-energy subtraction chest radiography. In conclusion, a dose reduction of approximately 25 % compared to the conventional method can be achieved. The limitations are the shape of the simulated mass and the use of chest phantom.

Section: RESEARCH PAPER

Keywords: Chest radiography; X-ray; U-net; deep learning; flat panel detector

Citation: Shu Onodera, Yongbum Lee, Tomoyoshi Kawabata, Dose reduction potential in dual-energy subtraction chest radiography based on the relationship between spatial-resolution property and segmentation accuracy of the tumor area, Acta IMEKO, vol. 11, no. 2, article 28, June 2022, identifier: IMEKO-ACTA-11 (2022)-02-28

Section Editor: Francesco Lamonaca, University of Calabria, Italy

Received September 30, 2021; **In final form** February 23, 2022; **Published** June 2022

Copyright: This is an open-access article distributed under the terms of the Creative Commons Attribution 3.0 License, which permits unrestricted use, distribution, and reproduction in any medium, provided the original author and source are credited.

Corresponding author: Shu Onodera, e-mail: onodera@rad.hosp.tohoku.ac.jp

1. INTRODUCTION

Chest radiography is the most basic diagnostic imaging procedure for lung diseases. However, the amount of X-rays that the patient is exposed to is enormous, including in the case of standing position imaging which is usually performed during medical examinations and bedside imaging for critically ill patients [1]. Compared with computed tomography (CT) examination, which provides three-dimensional information, the amount of exposure in radiography is very low (CT: 10 mSv, chest radiography: 0.1 mSv) [2]-[5] and its importance in terms of convenience of examination cannot be underestimated.

Usually, a high voltage of approximately 120 kV is applied during chest radiography to emphasize the contrast of the lung field rather than that of the ribs [6]. Nevertheless, the shadow of the rib remains on the image, making it difficult to detect the shadow of the soft tissue that overlaps that of the ribs. To address this problem, it has been developed an energy subtraction process [7] in which two types of image data with different radiographic energy characteristics are obtained with a single exposure, the bone shadows are removed through weighed differentiation of the respective images, and the image of the soft tissue alone is segmented (hereinafter, referred to as soft tissue imaging). Once bone shadows are removed, it becomes easier to detect tumours in soft tissue images. However, because the image quality in chest radiography considerably varies for

different parts due to factors such as the amount of radiation reaching the detector and the amount of scatter radiation, detectability may differ depending on the location of the tumour. In particular, the scatter radiation generated from the clavicle and scapula is believed to significantly affect the upper lobe of the lung, which is a common site of adenocarcinoma [8]. The spatial-resolution property of the image is also a very important factor in tumour detection [9]. The spatial-resolution property is a measure of the sharpness of an image and is an important characteristic that determines the detectability of lesions in X-ray images. Chest radiography images are generally subjected to several image-processing techniques to improve image quality, and these processing tools lead to a nonlinear behaviour that depends on image quality, which is different for different parts [10]. Thus, the quality of the soft tissue image also shows nonlinear behaviour, and task-based evaluation in a measurement environment that reflects clinical conditions is necessary to determine the spatial-resolution property.

The use of computer-aided diagnosis (CAD) in diagnostic imaging has increased [11], [12]. Earlier, image interpretation was performed by radiologists, based on their cultivated experience. However, with the recent increase in the use of radiography and the consequent increase in the number of images, CAD was introduced to reduce the burden on radiologists. CAD based on deep learning has been attracting attention recently, and it may soon be possible to detect a tumour even in a low-dose image with high noise.

In previous reports on energy subtraction-treated chest radiographs, visual evaluations of images acquired by the computed radiography (CR) systems have been reported [13]-[17]. The purpose of this study was to investigate the relationship between the spatial-resolution property of soft tissue images obtained by the flat panel detector (FPD) system and the lesion detection ability based on deep learning and explore the possibility of dose reduction during energy subtraction chest radiography.

2. MATERIALS AND METHODS

2.1. Image acquisition

An acrylic cylindrical simulated tumour with a diameter of 20 mm and thickness of 3 mm was placed in four regions on the chest phantom (right supraclavicular, left middle lung, right lower lung, and mediastinum), Figure 1.

Bone structure such as the clavicle, shoulder blade, and ribs as well as soft tissues as the mediastinum and pulmonary vascularity are located in the chest phantom. The single-exposure dual-energy subtraction system, [18], [19] CALNEO Dual (FUJIFILM Medical Co. Ltd. Tokyo, Japan, with a pixel size of 0.15 mm), was used in this study. The FPD implemented in this

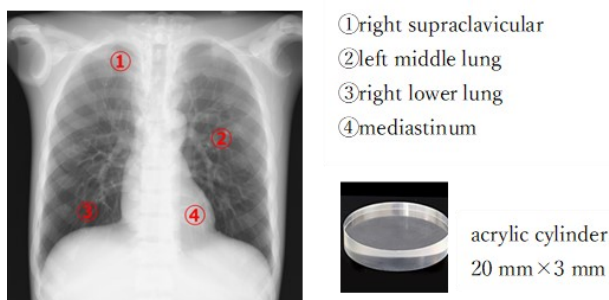


Figure 1. Phantom image and placement of acrylic cylinder.

Table 1. Imaging conditions.

Source image distance in cm	Field size in cm	Tube voltage in kV	Image depth in bit	Dose in mA s
180	43.2	115	12	1.6 (reference)
				1.2 (25 % down)
				0.8 (50 % down)

system consisted of two stacked scintillators. Normal energy images were collected in the first layer (cesium iodide scintillator), and the second layer (gadolinium sulfide scintillator) collected high-energy images transmitted through the first layer. Table 1 lists the imaging conditions used. The source-image distance was fixed at 180 cm, the field size was 43.2 cm, the image depth was 12 bits, and the tube voltage was 115 kV. Three types of imaging doses were used: a standard dose of 1.6 mA s, which was then reduced by 25 % to 1.25 mA s and then reduced by 50 % to 0.8 mA s, and 100 images of each type were acquired.

2.2. Calculation of the spatial-resolution property

Chest radiography images are generally subjected to several image-processing techniques to improve image quality. Frequency-processing and dynamic-range compression processing are typical examples. However, these processing tools lead to a nonlinear behaviour that depends on image quality, which is different for different parts. Therefore, in this study, the spatial-resolution property was determined by task-based evaluation, and the task-based modulation transfer function (TTF) was computed as its index [20]. The TTF calculation process is shown in Figure 2. The edge spread function (ESF) for the cylinder was obtained by averaging the profiles that cross the edge of the cylinder, measured from the centre in the direction of radiation. Next, TTF was calculated using the Fourier transform of the line spread function obtained by differentiating the ESF. One of the factors to be considered when determining the TTF of a soft tissue image is the signal-to-noise ratio (SNR) of the image. Because images with a low SNR create large errors in the calculation results, in this study, the image without acrylic was subtracted from the image with acrylic, and an image with a high SNR was created through the additive average of 100 such images, which was then used to calculate the TTF (Figure 3).

2.3. Building the deep learning environment

CAD using deep learning has been an area of active research in recent years and has a wide range of applications in medical

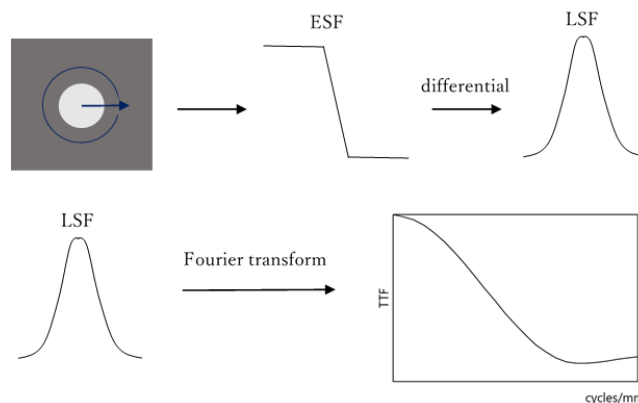


Figure 2. TTF calculation process.

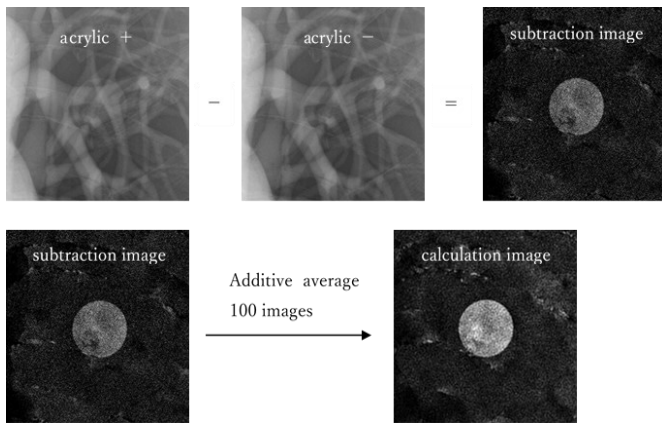


Figure 3. Creating the TTF calculation image.

imaging, such as lesion detection, area extraction, and image noise reduction. Image segmentation refers to the process of dividing an image into regions corresponding to each object. Because the target areas in medical imaging are organs or lesions, the positional information must be specified in the original input

image at the time of segmentation. U-net [21] is a typical example of a deep convolutional neural network for image segmentation. The present study deals with the detection of lung tumours using U-net in soft tissue images. Figure 4 shows the structure of the U-net used in this study. The usage environment of U-net in this research is as follows: OS: Windows10, Framework: Python3.7, TensorFlow, Keras, CPU: Core i7-10750H, Memory: 16G. The ReLu function and sigmoid function were used as activation functions, cross entropy as the loss function, and Adam as the learning optimization algorithm.

2.4. Data set for deep learning

The acquired soft tissue image (window width: 8500, window level: 8100, 14 bits) was segmented into 128×128 pixels centred around the tumour and converted to png format (window width: 255, window level: 128, 8bits). Fifty standard-dose images were input in U-net as training data and 50 reduced-dose images as evaluation data, and learning was conducted by setting the number of epochs to 30. The teaching data for the soft tissue images containing the tumour were created by binarizing the image into the tumour area and other areas (Figure 5).

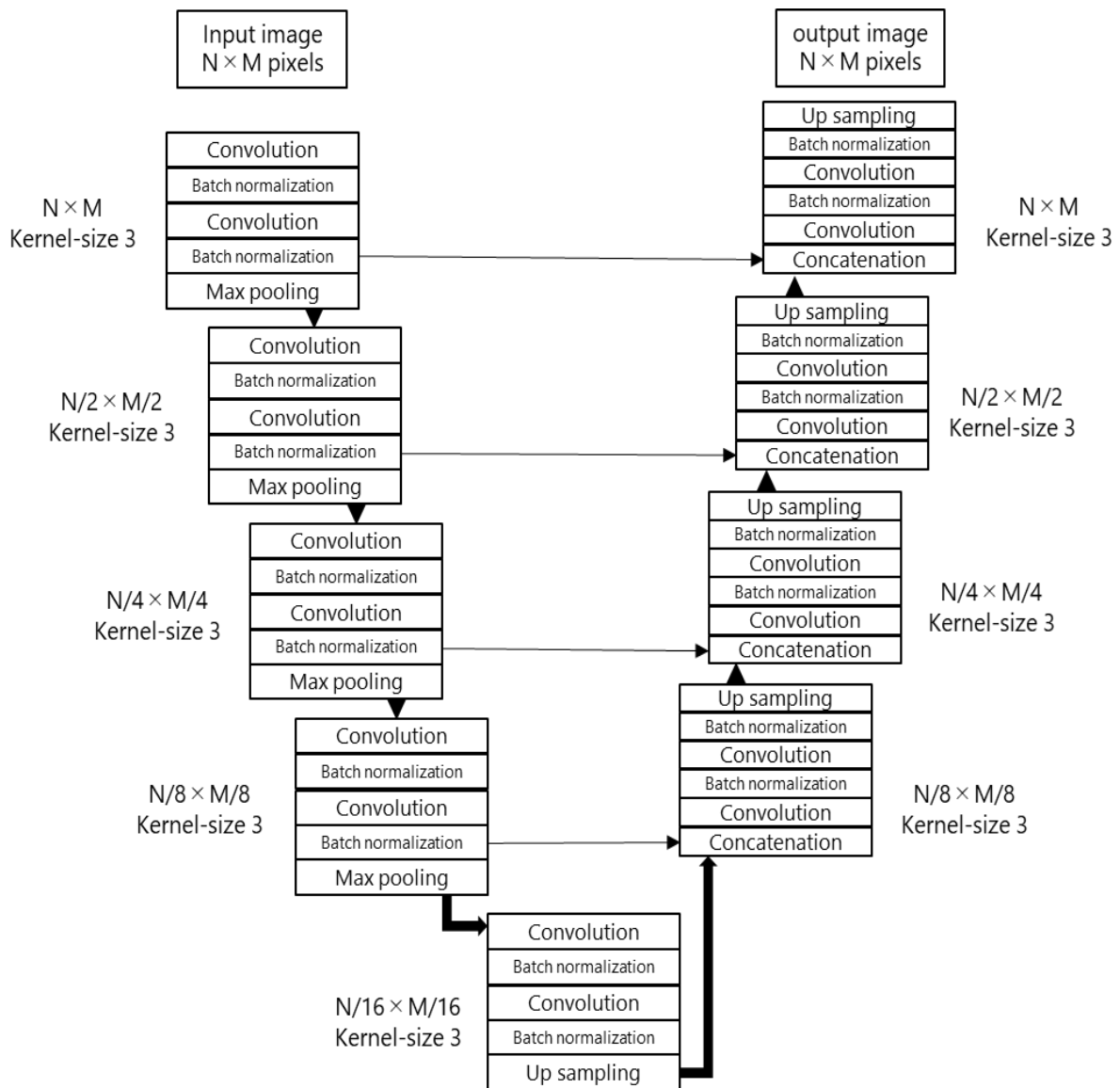


Figure 4. The structure of the U-net in this study.



Figure 5. Creation of teaching data.

2.5. Evaluation of the segmented tumour area

The Dice coefficient [22] was calculated as the degree of similarity between the output image and the teacher image to evaluate the extraction accuracy of the tumour region using U-net. The Dice coefficient is defined by the following formula:

$$Dice(A, B) = \frac{2|A \cap B|}{|A| + |B|}. \quad (1)$$

Here, A denotes the tumour region in the teaching image (region with a digital value of 255), and B denotes the tumour region in the output image (region with a digital value of 255).

2.6. Evaluation of the correlation between spatial-resolution property and segmentation accuracy of tumor area

In this study, the correlation between the spatial-resolution property of each dose image and the segmentation accuracy of the tumour area in the four regions where the tumour was placed was evaluated using linear regression analysis. A scatter plot was created by treating the TTF and Dice coefficient of each dose image from 0.2 to 1.2 cycle/mm (intervals of 0.2 cycle/mm) as variables. The Dice coefficient for the reference dose image was set to 1.

3. RESULTS

Figure 6 shows the TTF results for each condition. No difference was observed between the TTFs of the reference dose image and the 75 % dose image in the supraclavicular region, where the contrast was low due to the influence of scattered

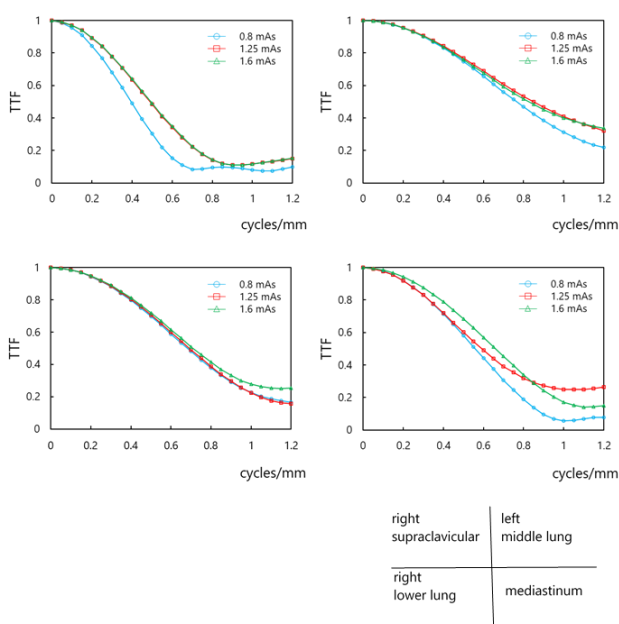


Figure 6. TTFs for each condition.

Table 2. Dice coefficients for each of the conditions.

mA s	Right supraclavicular	Left middle lung	Right lower lung	Mediastinum
1.25	0.960	0.960	0.959	0.971
0.8	0.937	0.969	0.963	0.967

radiation from the thoracic spine, clavicle, and scapula; however, the similarity decreased significantly in the TTF of 50 % dose images. In contrast, in the middle and lower lung regions where the effect of scattered radiation was small and the contrast was high compared to the supraclavicular region, the TTFs were generally high and the difference in values between doses was small. In the mediastinum, TTFs were low as in the supraclavicular region because of the low contrast due to the scattered radiation from the heart and sternum, but the decrease was not as high as that in the supraclavicular region; in comparison, the TTF in the supraclavicular region was the lowest among all the other regions.

Table 2 shows the average values of the Dice coefficients of the 50 datasets for each condition. The Dice coefficient between the segmented tumour area and the teaching data in the 75 % dose image showed a generally high value of approximately 0.96, regardless of the location of the tumour. Furthermore, the TTF of the 75 % dose image showed a value similar to that of the reference dose image regardless of the location of the tumour. In contrast, the Dice coefficient in the 50 % dose image was as low as 0.937 when the tumour was located in the supraclavicular region. Likewise, the TTF of the 50 % dose image in which the tumour was located in the supraclavicular region showed a lower value compared to the reference dose image.

Figure 7 shows the actual tumour area segmented by U-net. In the 75 % dose condition, the segmented images were highly similar to the teaching data, regardless of the location of the tumour. However, in the 50 % dose condition and when the tumour was located in the right supraclavicular region, the segmented region was slightly larger compared with the teaching data. Figure 8 to Figure 11 show the correlation between TTF and Dice coefficient in soft tissue images. A positive correlation was observed between the TTF and Dice coefficient of every dose image at all spatial frequencies in the right supraclavicular and the right lower lung regions and between the frequencies of 0.2 to 0.8 cycle / mm in the mediastinum section. In contrast, no correlation was observed between the TTF and Dice coefficients in any of the spatial frequencies in the left middle lung region.

4. DISCUSSION

In the case of the simulated tumour located in the right supraclavicular region and under 50 % dose, both the TTF and Dice coefficients showed significantly low values. One reason for this could be that the contrast of the tumour was reduced by scattered radiation mainly from the clavicle and scapula due to the complicated bone structure of the supraclavicular region. A second reason could be the fact that the tumour area could not be segmented accurately because of the increased image noise because the amount of radiation reaching the detector was smaller than that reaching other parts.

In the case in which the simulated tumour was located in the mediastinum region, the value of TTF was not very different from that when the tumour was in the middle and lower lung regions, and the Dice coefficient also showed a similar value. In the mediastinum region, the amount of radiation reaching the detector was less than that of the middle and lower lung regions,

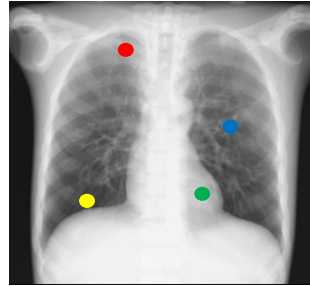
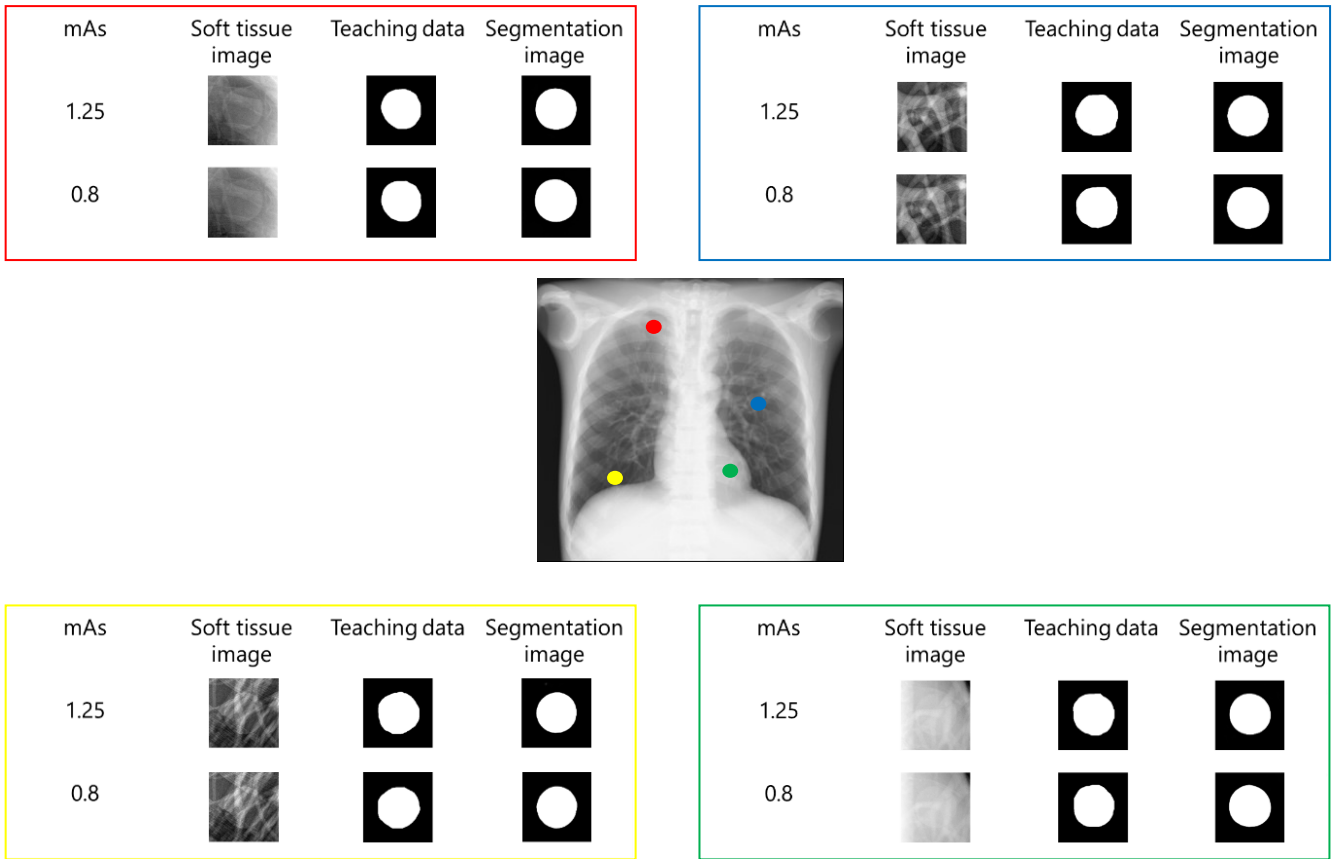


Figure 7. Mass region segmentation using for each of the conditions.

and the amount of scattered radiation from the sternum and heart was also large. Therefore, under the 50 % dose condition, the TTF and Dice coefficients were perceived to be as low as the right supraclavicular region. However, as the tumour in this area had fewer pulmonary blood vessels around it than other sites, the

structure was relatively simple and the tumour area could be segmented accurately (Figure 12).

The results of this study show that there is a high degree of correlation between the spatial resolution of the soft tissue image and the segmentation accuracy of the tumour area using deep

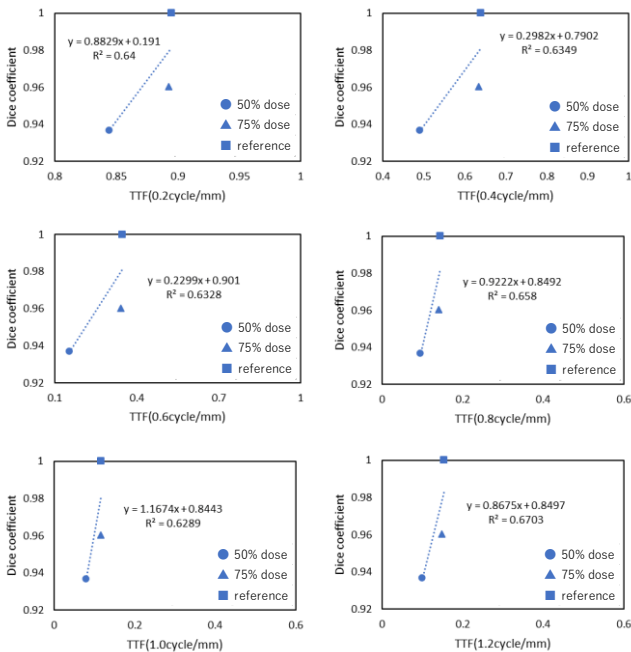


Figure 8. Between TTF and dice coefficient (right supraclavicular).

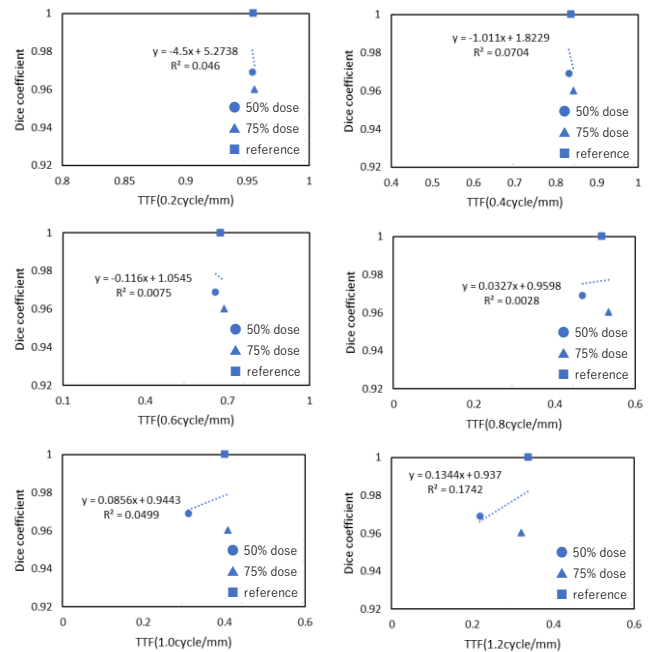


Figure 9. Between TTF and dice coefficient (left middle lung).

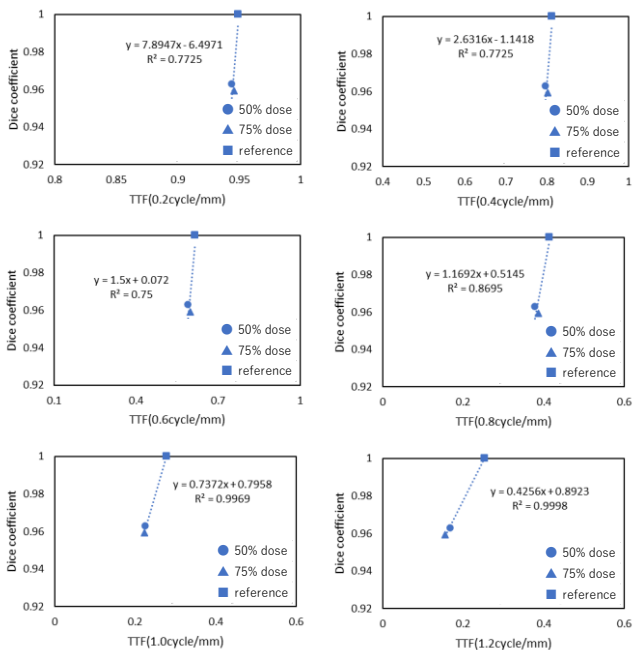


Figure 10. Between TTF and dice coefficient (right lower lung).

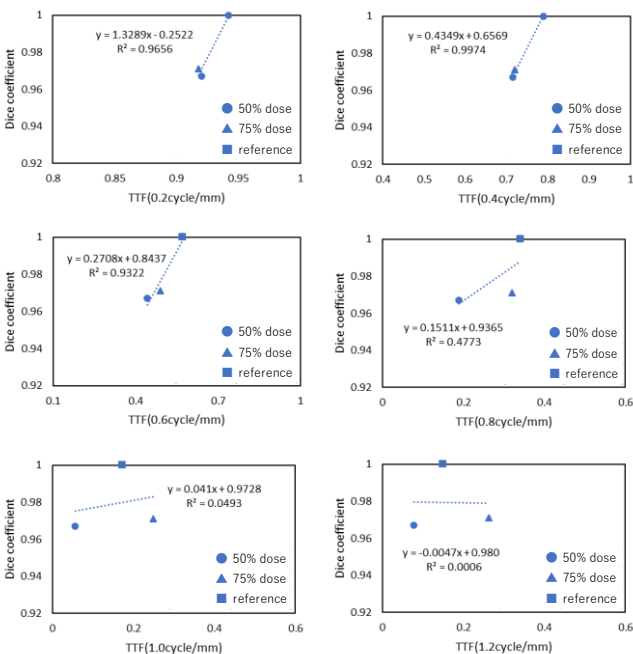


Figure 11. Between TTF and dice coefficient (mediastinum).

learning in the supraclavicular, lower lung, and mediastinum regions. In the 75 % dose images, the TTF was high regardless of the tumour location, and the Dice coefficient was also high. In contrast, in the 50 % dose images, when the tumour was present in the supraclavicular region, the TTF was significantly reduced, and the Dice coefficient was also low. In other words, if the radiation dose is reduced to 50 % of the conventional radiation condition, tumour that develop in the supraclavicular region may not be segmented accurately due to a decrease in TTF. No correlation was confirmed between TTF and the Dice coefficient in the middle lung area. This could be because there was no difference in TTFs of the dose images between 0.2 and 0.6 cycle / mm, and between the 0.8 and 1.2 cycle / mm, there

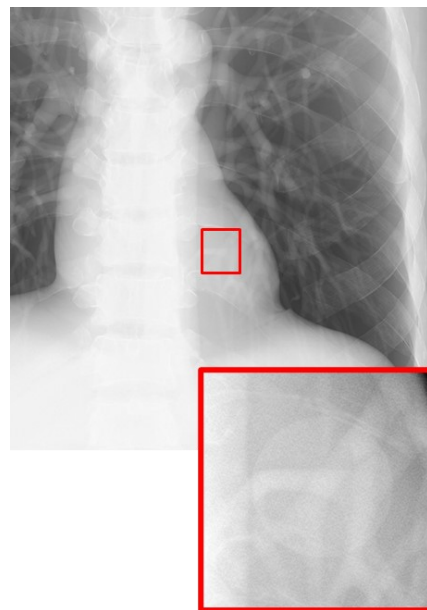


Figure 12. Pulmonary vessels around the mass in the mediastinum.

was no difference in the TTFs of the 75 % dose image and the reference dose image. Among the four sites examined in this study, the highest amount of radiation reached the detector from the middle lung area, and the amount of scattered radiation from the surroundings was also small. Therefore, no correlation could be confirmed between the TTF and the Dice coefficient in the middle lung region, and the Dice coefficients of all dose images showed a high value of approximately 0.96. The discussion above suggests that, with single-exposure dual-energy subtraction chest radiography by the FPD system, it may be possible to reduce the dose by approximately 25 % compared to the conventional method.

Figure 13 shows the detection quantum efficiency (DQE) in the radiation qualities of the RQA9 of the CR system, which was manufactured by the same company as the CALNEO Dual system used in this study [23], [24]. Because lung tumors are the targets of this study, we focused on the value of the spatial frequency of 1 cycle / mm [25]. The DQE value at 1 cycle / mm is approximately 0.5 for the CALNEO Dual and about 0.2 for the CR system, respectively, and the detection quantum efficiency of the CALNEO Dual is approximately 2.5 times higher. A system with an excellent DQE has a high degree of freedom in adjusting the balance between sharpness and graininess through image processing [26]. Therefore, selecting

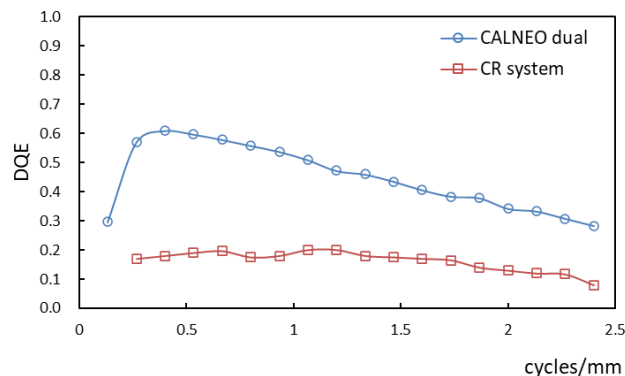


Figure 13. DQE for CALNEO dual and CR system with RQA9 spectra.

parameters with good spatial-resolution properties for multi-frequency processing in single-exposure dual-energy subtraction chest radiography using FPD could lead to further dose reduction.

As a limitation of this study, we would first mention the structure of the simulated tumors. In this study, an acrylic material with a simple cylindrical structure was used as the simulated tumor. Actual lesions with increased malignancy, such as spiculated lesions, often have more complex structures, and in such cases, the results may differ. Moreover, in this study, all measurements from beginning to end were performed using a phantom, and the effects of heartbeat, which is a major problem in actual clinical practice, [27] have not been considered. However, to reduce the effects of heartbeat, the imaging time was shortened to the largest extent possible, and measurements were performed in a very short interval of approximately 10 ms, as is done in clinical practice; hence, we hope that the results will not be greatly affected.

5. CONCLUSIONS

In this study, we clarified the relationship between the spatial resolution of single-exposure dual-energy subtraction chest radiography using the FPD system and the segmentation accuracy of the tumour area using deep learning. The TTFs of the reference dose image and the 75 % dose image showed almost the same frequency characteristics regardless of the location of the tumour, and the Dice coefficient also showed a high value. When the tumour was located in the right supraclavicular region and under 50 % dose, the frequency characteristics were significantly reduced, and the Dice coefficient was also low. Therefore, a close relationship between the spatial-resolution property and the segmentation accuracy of the tumour area was confirmed using deep learning in single-exposure dual-energy subtraction chest radiography using the FPD system, and it may be possible to achieve dose reduction of approximately 25 % compared to the conventional method.

REFERENCES

- [1] UNSCEAR. Medical Radical Exposures. Sources and Effects of Ionizing Radiation, UNSCEAR 2008 Report. New York: United Nations; 2010. Annex A.
- [2] L. J. M. Kroft, L. van der Velden, I. H. Girón, J. J. H. Roelofs, A. de Roos, J. Geleijns, Added value of ultra-low-dose computed tomography, dose equivalent to chest X-ray radiography, for diagnosing chest pathology, *J. Thorac Imaging*, 34 (2019), pp. 179-186.
DOI: [10.1097/RTI.0000000000000404](https://doi.org/10.1097/RTI.0000000000000404)
- [3] R. Ward, W. D Carrol, P. Cunningham, S. A Ho, M. Jones, W. Lenney, D. Thonpson, F. J Gilchrist, Radiation dose from common radiological investigations and cumulative exposure in children with cystic fibrosis: An observational study from a single UK centre, *Observational Study*, 7 (2017), pp. 1-5.
DOI: [10.1136/bmjopen-2017-017548](https://doi.org/10.1136/bmjopen-2017-017548)
- [4] S. Singh, M. K. Kalra, R. D. Ali Khawaja, A. Padle, S. Pourjabbar, D. Lira, J. A. O. Shepard, S. R. Digumarthy, Radiation dose optimization and thoracic computed tomography, *Radiol. Clin. North Am.*, 52(2014), pp. 1-15.
DOI: [10.1016/j.rcl.2013.08.004](https://doi.org/10.1016/j.rcl.2013.08.004)
- [5] International Commission on Radiological Protection, The 2007 Recommendations of the International Commission on Radiological Protection, ICRP Publication 103, *Ann. ICRP* 37 (2-4).
- [6] O. W. Hamer, C. B. Sirlin, M. Strotzer, I. Borisch, N. Zorger, S. Feuerbach, M. Volk, Chest radiography with a flat-panel detector:

Image quality with dose reduction after copper filtration. *Radiology*, 237 (2005), pp- 691-700.
DOI: [10.1148/radiol.2372041738](https://doi.org/10.1148/radiol.2372041738)

- [7] M. Fukao, K. Kawamoto, H. Matsuzawa, O. Honda, T. Iwaki, T. Doi, Optimization of dual-energy subtraction chest radiography by use of a direct-conversion flat-panel detector system, *Radiol Phys Technol*, 8 (2015), pp. 46-52.
DOI: [10.1007/s12194-014-0285-y](https://doi.org/10.1007/s12194-014-0285-y)
- [8] K. Honda, Y. Matsui, H. Imai, Regional distribution of lung cancer, *Haigan*, 23 (1983), pp. 11-21.
- [9] Y. Fujimura, H. Nishiyama, T. Masumoto, S. Kono, Y. Kitagawa, T. Ikeda, T. Furukawa, T. Ishida, Investigation of reduction of exposure dose in digital mammography: Relationship between exposure dose and image processing, *JpnSoc, Nihon Hoshasen Gijutsu Gakkai Zasshi*, 64(2008), pp. 259-267.
DOI: [10.6009/jirt.64.259](https://doi.org/10.6009/jirt.64.259)
- [10] K. Kishimoto, E. Ariga, R. Ishigaki, M. Imai, K. Kawamoto, K. Kobayashi, M. Sawada, K. Noto, M. Nakamae, R. Higashide, Study of appropriate dosing in consideration of image quality and patient dose on the digital radiography, *JpnSoc, Nihon Hoshasen Gijutsu Gakkai Zasshi*, 67(2011), 1381-1397.
DOI: [10.6009/jirt.67.1381](https://doi.org/10.6009/jirt.67.1381)
- [11] K. Doi, Current status and future potential of computer-aided diagnosis in medical imaging, *Br J Radiol*, 78 (2005), Spec No 1, S3-S19.
DOI: [10.1259/bjr/82933343](https://doi.org/10.1259/bjr/82933343)
- [12] H. Fujita, Present status of mammography CAD system, *Med Imaging Technol*, 1 (2003), 27-33.
- [13] S. Kido, J. Ikezoe, H. Naito, J. Arisawa, S. Tamura, T. Kozuka, W. Ito, K. Shimura, H. Kato, Clinical evaluation of pulmonary nodules with single-exposure dual-energy subtraction chest radiography with an iterative noise-reduction algorithm, *Radiology*, 194 (1995), pp. 407-412.
DOI: [10.1148/radiology.194.2.7824718](https://doi.org/10.1148/radiology.194.2.7824718)
- [14] S. Kido, K. Kuriyama, N. Hosomi, E. Inoue, C. Kuroda, T. Horai, Low-cost soft-copy display accuracy in the detection of pulmonary nodules by single-exposure dual-energy subtraction: comparison with hard-copy viewing, *J Digit Imaging*, 2000, pp. 33-37.
DOI: [10.1007/BF03168338](https://doi.org/10.1007/BF03168338)
- [15] J. R. Wilkie, M. L. Giger, M. R. Chinander, T. J. Vokes, R. M. Nishikawa, M. D. Carlin, Investigation of physical image quality indices of a bone densitometry system, *Med Phys*, 31 (2004), pp. 873-881.
DOI: [10.1118/1.1650528](https://doi.org/10.1118/1.1650528)
- [16] S. Kido, H. Nakamura, W. Ito, K. Shimura, H. Kato, Computerized detection of pulmonary nodules by single-exposure dual-energy computed radiography of the chest (Part 1), *Eur J Radiol*, 44(2002), 198-204.
DOI: [10.1016/s0720-048x\(02\)00268-1](https://doi.org/10.1016/s0720-048x(02)00268-1)
- [17] S. Kido, K. Kuriyama, C. Kuroda, H. Nakamura, W. Ito, K. Shimura, H. Kato, Detection of simulated pulmonary nodules by single-exposure dual-energy computed radiography of the chest: Effect of a computer-aided diagnosis system (Part 2), *Eur J Radiol*, 44 (2002), pp. 205-209.
DOI: [10.1016/s0720-048x\(02\)00269-3](https://doi.org/10.1016/s0720-048x(02)00269-3)
- [18] L. Shi, M. Lu, N. R. Bennett, E. Shapiro, J. Zhang, R. Colbeth, J. S. Lack, A. S. Wang, Characterization and potential applications of a dual-layer flat-panel detector, *Med Phys*, 47(2020), Epub 2020 May 18, pp. 3332-3343.
DOI: [10.1002/mp.14211](https://doi.org/10.1002/mp.14211)
- [19] M. Lu, A. Wang, E. Shapiro, A. Shiroma, J. Zhang, J. Steiger, J. S. Lack, Dual energy imaging with a dual-layer flat panel detector, *SPIE Med Imaging;10948 Physics of Medical Imaging*, Sandiego, United States, 2019
DOI: [10.1117/12.2513499](https://doi.org/10.1117/12.2513499)
- [20] S. Richard, D. B. Husarik, G. Yadava, S. N. Murphy, E. Samei, Towards task-based assessment of CT performance: System and object MTF across different reconstruction algorithms, *Med Phys*, 39(2012), 4115-4122.
DOI: [10.1118/1.4725171](https://doi.org/10.1118/1.4725171)

- [21] O. Ronneberger, P. Fischer, T. Brox, U-net: Convolutional networks for biomedical image segmentation Lecture Notes in Computer Sciences (including SubserLect Notes ArtifIntellLect Notes Bioinformatics). 2015; 9351: pp. 234-241.
- [22] B. Sahiner, A. Pezeshk, L. M. Hadjiiski, X. Wang, K. Drukker, K. H. Cha, R. M. Summers, M. L. Giger, Deep learning in medical imaging and radiation therapy. *Med Phys*, 46(2019), Epub 2018 Nov 20, e1-e36.
DOI: [10.1002/mp.13264](https://doi.org/10.1002/mp.13264)
- [23] IEC. 62220-1. Medical Electrical Equipment-Characteristics of Digital X-Ray Imaging Devices part 1: Determination of Detective Quantum Efficiency. International Electrotechnical Commission; 2003.
- [24] IEC. 62220-1-2. Medical Electrical Equipment-Characteristics of Digital X-Ray Imaging Devices part 1-2: Determination of Detective Quantum Efficiency-Detectors Used in Mammography. International Electrotechnical Commission; 2007.
- [25] T. Yokoi, T. Takata, K. Ichikawa, Investigation of image quality identification utilizing physical image quality measurement in direct- and indirect-type of flat panel detectors and computed radiography, *Nihon Hoshasen Gijutsu Gakkai Zasshi*, 67(2011), pp. 1415-1425.
DOI: [10.6009/jjrt.67.1415](https://doi.org/10.6009/jjrt.67.1415)
- [26] A. R. Cowen, A. G. Davies, M. U. Sivananthan, The design and imaging characteristics of dynamic, solid-state, flat-panel x-ray image detectors for digital fluoroscopy and fluorography, *Clin Radiol*, 63(2008), 1073-1085.
DOI: [10.1016/j.crad.2008.06.002](https://doi.org/10.1016/j.crad.2008.06.002)
- [27] European Commission, CHEST. (LUNGS AND HEART) PA and Lateral Projections. European Guidelines on Quality Criteria for Diagnostic Radiographic Image. EUR. Luxembourg: CEC; 1996:12:16260 EN.